

Robustness of Quantum Chaos and Anomalous Relaxation in Open Quantum Circuits

Takato Yoshimura^{1,2,*} and Lucas Sá^{3,4,†}

¹All Souls College, Oxford OX1 4AL, U.K.

²Rudolf Peierls Centre for Theoretical Physics, University of Oxford, 1 Keble Road, Oxford OX1 3NP, U.K.

³TCM Group, Cavendish Laboratory, University of Cambridge, JJ Thomson Avenue, Cambridge CB3 0HE, U.K.

⁴CeFEMA, Instituto Superior Técnico, Universidade de Lisboa, Av. Rovisco Pais, 1049-001 Lisboa, Portugal

Dissipation is a ubiquitous phenomenon in nature that affects the fate of chaotic quantum dynamics. To characterize the interplay between quantum chaos and dissipation in generic quantum many-body systems, we consider a minimal dissipative Floquet many-body system. We study the dissipative form factor (DFF), an extension of the spectral form factor to open quantum systems, of the random phase model in the presence of arbitrary one-site nonunitary gates (quantum channels). In the limit of large local Hilbert space dimension, we obtain an exact expression for the DFF averaged over the random unitary gates, with simple, closed-form expressions in the limit of large times. We find that, for long enough times, the system always relaxes (i.e., the DFF decays) with two distinctive regimes characterized by the presence or absence of gap closing. While the system can sustain a robust ramp for a long (but finite) time interval in the gap-closing regime, relaxation is “assisted” by quantum chaos in the regime where the gap remains nonzero. In the latter regime, we find that, if the thermodynamic limit is taken first, the gap does not close even in the dissipationless limit.

Introduction.—Quantum chaos is a powerful statistical framework for studying generic complex many-body quantum systems in and out of equilibrium. Relating the universal late-time dynamics and typical observables of such systems to statistical properties of random matrices allows for a better theoretical understanding of issues ranging from thermalization in statistical mechanics [1, 2], to information scrambling in quantum information science [3–5], and the holographic principle in quantum gravity [6–9]. In closed quantum systems with unitary dynamics, the spectral form factor (SFF) [9–14] assumes a particularly crucial role, as it establishes a concrete connection between dynamics and spectral correlations [15–21]. In this context, the repulsion of eigenvalues and spectral rigidity of the spectra of ergodic systems manifest as the presence, at late times, of a ramp in the SFF, one of the hallmark signatures of quantum chaos.

Random quantum circuits (RQCs) [22–32] provide an excellent platform to investigate the out-of-equilibrium dynamics and quantum chaos features of local strongly interacting quantum systems, due to their analytical tractability (sometimes only in the limit of large Hilbert space dimension q [24, 25]), simple numerical implementation, and simulability in emergent quantum computing platforms [33]. In particular, the emergence of the ramp and deviations from random-matrix universality can be analytically understood in a particular family of Floquet RQCs, the random phase model (RPM) [25, 34, 35], where the exact SFF was computed at $q \rightarrow \infty$ [25].

By now, much is known about unitary circuits and pure-state dynamics, even in the presence of external measurements [32, 36–42]. Nevertheless, present-day quantum computers are noisy, which makes it important to study nonunitary dissipative circuits, implemented by lossy or imperfect hardware, and modeled by quantum-channel gates (the dissipative generalization of unitary

gates) [43–52]. More broadly, all physical systems are, to some degree, influenced by interactions with an environment or errors in controlling protocols and it is, therefore, of great importance to test the robustness of quantum chaotic features in the presence of dissipation and quantify the dissipative corrections to the quantities most commonly used to characterize chaos, e.g., the ramp of the SFF, the butterfly velocity [22, 23, 53], or the quantum Lyapunov exponent [8, 54].

Previous research in similar directions has focused on the entanglement dynamics and information scrambling in brickwork open RQCs [45–50], but the spectral correlations and relaxation dynamics of dissipative Floquet circuits have remained unexplored. Distinct open-system extensions of the SFF have been proposed that capture different aspects of dissipative quantum chaos [55–67]. In particular, the dissipative form factor (DFF) [55] extends the dynamical definition of the SFF and is given by the trace of the quantum channel. The late-time behavior of the DFF is controlled by the spectral gap and was used to compute it for random Liouvillians [55], while the finite-time behavior captures dynamical phase transitions [56]. It does not, however, measure the correlations of eigenvalues in the complex plane, which are captured, instead, by a different quantity, the dissipative spectral form factor [58–63]. This motivates us to ask a fundamental question: What, if any, are the universal features of the DFF in quantum chaotic systems?

To take a step forward in answering this question, in this Letter, we introduce a minimally-structured many-body chaotic open quantum system using a dissipative extension of the RPM, which we dub the dissipative random phase model (DRPM). To test the robustness of the chaotic dynamics against the presence of dissipation, we analytically compute its DFF for arbitrary on-site dissipation in the limit of large local Hilbert space dimension.

We find that, when dissipation is weak enough, the ramp, which signals the presence of level repulsion and spectral rigidity, persists over a timescale that is parametrically larger than the Thouless time, before the DFF finally decays exponentially at a rate set by the spectral gap. Remarkably, the gap does not necessarily close in the limit of vanishing dissipation if the thermodynamic limit is taken first, a phenomenon recently unveiled in several dissipative many-body systems [68–71] and dubbed anomalous relaxation [69]. Our results further support the conjecture that anomalous relaxation is a result of the underlying quantum chaos.

The model.—The dynamics of the DRPM is generated by the Floquet operator of the RPM and on-site dissipation prescribed by quantum channels. Let us start by recalling the definition of the RPM [25]. We consider a spin chain of L sites where the on-site Hilbert space dimension is $q \in \mathbb{Z}^+$. The time-evolution of the model is discrete and governed by the Floquet operator $W(t) = W^t$ where the operator W is made of two layers $W = W_2 W_1$. First, $W_1 = U_1 \otimes \dots \otimes U_L$ consists of $q \times q$ on-site random unitaries U_x that are Haar distributed. Second, W_2 induces interactions among adjacent sites and acts on the basis state $|a_1\rangle \otimes \dots \otimes |a_L\rangle \in (\mathbb{C}^q)^L = \mathcal{H}$ diagonally with the phase $\exp\left(i \sum_{x=0}^L \varphi_{a_x, a_{x+1}}\right)$. Each $\varphi_{a_x, a_{x+1}}$ is independently Gaussian distributed with mean zero and variance $\varepsilon/2 > 0$.

In the DRPM, each Floquet step is followed by the action of the quantum channel Φ that describes local dissipation. In this Letter, we consider quantum channels that factorize into a product of decoupled single-site channels, i.e., $\Phi = \Phi_1 \otimes \dots \otimes \Phi_L$. The local quantum channel Φ_x acts on the state ρ_x at site x as $\Phi_x(\rho_x) = \sum_{i=0}^{k-1} M_i \rho_x M_i^\dagger$, where k is the number of channels and M_i are Kraus operators that satisfy $\sum_{i=0}^{k-1} M_i^\dagger M_i = I$, with I the identity (the channels at different sites $x = 1, \dots, L$ can be different). We normalize the Kraus operators as $q^{-1} \text{Tr}(M_i M_j^\dagger) = \eta_i \delta_{ij}$ for some $\eta_i > 0$. A complete time step of the nonunitary Floquet circuit is best represented as an operator on the doubled Hilbert space $\mathcal{H} \otimes \mathcal{H}^*$, which acts on the vectorized density operator as a matrix $\mathcal{W} = \Phi(W \otimes W^*)$. The entire circuit at time t is given by \mathcal{W}^t .

While the DFF can be computed exactly at large q for *any* quantum channel Φ_x as we demonstrate shortly, for definiteness, the example we fully work out is the DRPM where all Φ_x are the same fixed depolarizing channel, $\Phi_x(\rho_x) = (1-p)\rho_x + pI/q$, for which the Kraus operators are given by $M_0 = \sqrt{1-p(q^2-1)/q^2}I$ and $M_i = \sqrt{p/q^2}P_i$ ($i = 1, \dots, q^2-1$), where $0 \leq p \leq 1$ is the probability that the spin is depolarized (i.e., that its density matrix becomes the fully-mixed state I/q) and P_i are Hermitian operators that form a traceless orthonormal basis of on-site operators with $q^{-1} \text{Tr}(P_i P_j) = \delta_{ij}$. The normalization factor η_i for this channel is $\eta_0 =$

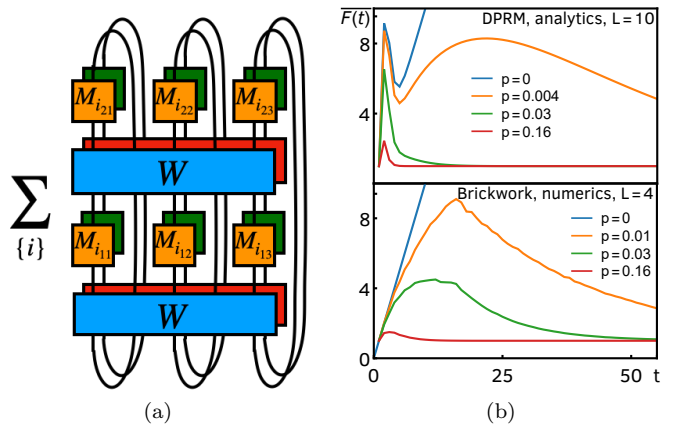


Figure 1. (a): Schematic representation of the computation of the DFF of the DRPM for $t = 2$ and $L = 3$. Blue and red gates represent the Floquet operator W and its conjugate W^* of the RPM. Yellow and green on-site gates are Kraus operators $M_{i,x,\tau}$ and their conjugate $M_{i,x,\tau}^*$. (b): DFF of Floquet open quantum circuits, for different values of p . Top panel: exact analytical result for the DRPM, Eq. (2), for $L = 10$ and $\varepsilon = 0.8$. Bottom panel: numerical results for a brickwork random Floquet circuit for $L = 4$ and $q = 2$.

$1 - p(q^2 - 1)/q^2 \approx 1 - p$ (where the approximate expression holds in the limit $q \rightarrow \infty$) and $\eta_i = p/q^3$, and the number of Kraus operators is $k = q^2$.

Exact DFF of the DRPM.—The central object in this Letter in understanding the effect of dissipation on quantum chaos is the DFF [55]. The DFF $F(t)$ was originally introduced for open quantum systems with a continuous time evolution described by a Lindbladian \mathcal{L} as $F(t) = \text{Tr} e^{t\mathcal{L}}$, where the Lindbladian is understood as the matrix acting on the doubled Hilbert space. Note that the DFF reduces to the standard SFF, $F(t) = |\text{Tr} e^{-iHt}|^2$, where H is the Hamiltonian, in the absence of dissipation. To generalize it to Floquet quantum circuits with discrete-time dynamics, we simply replace $e^{t\mathcal{L}}$ by the quantum channel \mathcal{W}^t of our circuit. Writing \mathcal{W}^t in the vectorized Kraus representation, $\mathcal{W}^t = \sum_{\underline{j}} K_{\underline{j}} \otimes K_{\underline{j}}^*$, with Kraus operators $K_{\underline{j}} = \prod_{\tau=1}^t \prod_{x=1}^L K_{j_{\tau x}}$ and $K_{j_{\tau x}} = M_{j_{\tau x}} W$ the Kraus operator at site x and time step τ , the DFF for the Floquet quantum circuit can be expressed as

$$F(t) = \sum_{\underline{j}} |\text{Tr} K_{\underline{j}}|^2. \quad (1)$$

See Fig. 1a for the diagrammatic representation of $F(t)$ with the system size $L = 3$. Interpreting $M_{j_{\tau x}}$ as a generalized measurement, the quantity $|\text{Tr} K_{\underline{j}}|^2$ is the SFF of a monitored (hybrid) quantum circuit [36–38], where at each site and point in time a depolarizing error can occur with probability p and the measurement outcome is recorded. We thus see that the DFF is the equal-weight average over all such possible measurement his-

tories, as relevant for an unmonitored quantum circuit (e.g., in the presence of an external environment or noise source), where one does not keep track of the measurement outcomes. In what follows, we evaluate the ensemble average of the DFF, Eq. (1), which we denote by $\overline{F}(t)$, at large q , where Haar-averaging becomes substantially simplified.

We follow the same strategy as in the computation of the SFF of the RPM [25], which is to calculate the DRPM diagrammatically; see the Supplemental material (SM) [72] for the details of the computation. Haar-averaging at each site induces local pairings of indices labeling on-site unitaries U_x and U_x^* , but it is straightforward to show that only those corresponding to cyclic pairings of indices contribute at $q \rightarrow \infty$, which is also the case in the SFF (in the SFF, these t pairings give rise to the late-time ramp $\sim t$) [25]. We label each pairing by $s = 0, \dots, t-1$ ($s=0$ corresponds to the pairing where both indices of U_x are contracted with those of U_x^* on the same time slice), and it turns out that diagrams associated with any $s \neq 0$ pairing carry the same factor $\kappa := \sum_i \eta_i^t$, while an $s=0$ pairing simply come with the factor 1 [72]. Since different pairings on two neighboring sites, a configuration which we call a *domain wall*, induce the statistical cost $e^{-\varepsilon t}$ upon averaging with respect to the phase φ , similarly to the SFF of the RPM [25], we find that the DFF of the DRPM at large q can be succinctly expressed as

$$\overline{F}(t) = \text{Tr} \hat{T}^L, \quad \hat{T} = TD, \quad (2)$$

where $T = (1 - e^{-\varepsilon t})I + e^{-\varepsilon t}E$ (E is the matrix completely filled with ones) is the $t \times t$ transfer matrix of the SFF and $D = \kappa I + (1 - \kappa)|0\rangle\langle 0|$ is the on-site dissipative contribution. Here $|s\rangle$ denotes the vector with a 1 in the s th coordinate and 0 elsewhere, thus $|s\rangle\langle s|$ is the projection matrix to the pairing labeled by s . The trace follows from periodic boundary conditions.

In Ref. [25], it was shown that the SFF of the RPM [corresponding to Eq. (2) at $\kappa = 1$: $\lim_{\kappa \rightarrow 1} \overline{F}(t) = \text{Tr} T^L$] displays a ramp for times larger than the Thouless time $t_{\text{Th}} = \varepsilon^{-1} \log L$. We are interested in how this behavior is modified by dissipation, which is quantified by the DFF. We emphasize that Eq. (2) is valid for any choice of local dissipative gate and all information on the latter is encoded in the weight κ . To make the analysis concrete, in the remainder of the paper, we focus on the depolarizing channel, i.e., $\kappa = (1-p)^t$ (in the large- q limit). The main features of the DFF are shown in Fig. 1b (top). After an initial peak (the Thouless peak), there is a linear ramp for $p=0$ (closed system), which is still sustained for small p and decays on a timescale set by the gap Δ . For larger p , the DFF decays immediately after the Thouless peak, and there is no ramp. We also numerically computed the DFF for a depolarizing qubit ($q=2$) brickwork random Floquet circuit (where the two-body unitary gates are Haar-distributed). We found the same behavior as in the

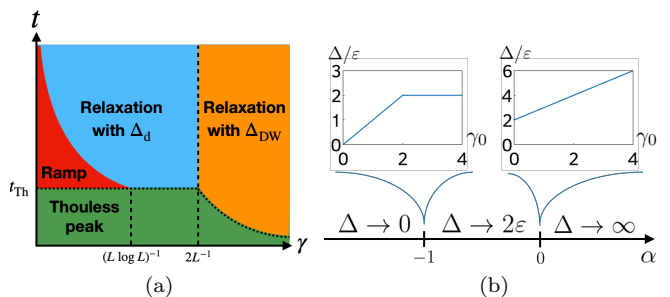


Figure 2. Relaxation in the DFF of the DRPM. (a): Different dynamical regimes in the DRPM. The boundary between the red and blue regions is given by t_d , while the dotted line separating the green region from the remaining ones corresponds to t_{DW} . (b) The large- L behavior of the gap for different α in $\gamma = \gamma_0 L^\alpha$. It is independent of γ_0 , except at the special points $\alpha = -1$ and $\alpha = 0$.

DRPM, see Fig. 1b (bottom). Although the circuit architecture is different and q is finite, we still observe the same qualitative behavior of the DFF (for this system size, the Thouless peak is absent). However, a detailed quantitative analysis of the timescales involved is complicated by the small system sizes available and we defer it to future work.

Relaxation in the DRPM.—As in generic open quantum systems, dissipation in the DRPM induces relaxation to the unique steady state, which is seen in the late-time exponential decay of the DFF to a constant plateau of value one. The most interesting question, however, is how the plateau is approached, which is summarized in Fig. 2.

We first notice that, after a sharp drop from the initial-time peak $\overline{F}(0) = q^{2L}$ to $\overline{F}(1) = 1$, the DFF develops a second peak (the Thouless peak, see Fig. 1b and the green region in Fig. 2a), which is a consequence of each site behaving independently at early times. This means that the early-time behavior of the DFF can be understood from a collection of single-site systems subject to dissipation. The DFF of the uncoupled single site (i.e., $\varepsilon = 0, L = 1$) dissipated by the depolarizing channel behaves as $1 + (t-1)\kappa$, thus the DFF of the DRPM at early times grows as $\overline{F}(t) \sim [1 + (t-1)\kappa]^L$.

At late times, the effect of the coupling between different sites sets in, thus inducing the decay of the Thouless peak, and the relaxation of the DFF. The late-time physics after the Thouless peak can be accurately approximated by the domain-wall expansion [72],

$$\overline{F}(t) \simeq 1 + t\kappa^L + tL\kappa e^{-2\varepsilon t} + \frac{t^2 L^2}{4} \kappa^L e^{-2\varepsilon t} + \dots, \quad (3)$$

where we only kept up to two domain walls, as they decay most slowly and hence capture the tail of the Thouless peak. The ellipsis refers to the terms containing more domain walls. It is convenient to introduce the effective dissipation strength $\gamma = -\varepsilon^{-1} \log(1-p) > 0$,

with which the asymptotics of Eq. (3) can be written as $\overline{F}(t) = 1 + K_d(t) + K_{\text{DW}}(t) + \dots$. Here, $K_d(t) = te^{-\gamma L \varepsilon t}$ is the direct contribution from dissipation, and shows an initial linear ramp, followed by an exponential decay at a rate $\Delta_d = \varepsilon \gamma L$. Instead, $K_{\text{DW}}(t) = tLe^{-\varepsilon t(2+\gamma)} + t^2 L^2 e^{-\varepsilon t(2+\gamma L)}/4$ describes the decay of the Thouless peak with the asymptotic gap $\Delta_{\text{DW}} = \varepsilon(2+\gamma)$. Note that the first term in $K_{\text{DW}}(t)$ becomes larger than the second term when $t \gg \log L/(\varepsilon \gamma L) =: t_*$. The overall asymptotic decay is set by the slower of these decay rates (the gap):

$$\Delta = \min\{\Delta_d, \Delta_{\text{DW}}\} = \min\{\varepsilon \gamma L, \varepsilon(2+\gamma)\}. \quad (4)$$

Below, we demonstrate how the competition between the decay of the Thouless peak and the ‘‘dissipation peak’’ induced by $K_d(t)$ amounts to a rich relaxation behavior. Since the relaxation timescales of the DRPM depend on the scaling of the parameter γ with L , we parameterize $\gamma = \gamma_0 L^\alpha$, where $\alpha \in \mathbb{R}$ and γ_0 is independent of L . In the following, we analyze in more detail the behavior of the DFF for different α , taking $L \rightarrow \infty$.

Robustness of the ramp.—We start with the case $\alpha < -1$, i.e., γ sufficiently small. In this regime, t_* diverges in the thermodynamic limit and, therefore, $K_{\text{DW}}(t)$ is always dominated by its second term at finite time. The Thouless peak (green region in Fig. 2a) thus decays over the timescale $t_{\text{DW}} = 2 \log L/[\varepsilon(2+\gamma L)] \simeq \varepsilon^{-1} \log L = t_{\text{Th}}$ and it is well-separated from, and occurs at a much earlier time than, the dissipation peak. In particular, the build-up of the dissipation peak can be thought of as a remnant of the ramp in the SFF, and the width of the peak can be arbitrarily stretched as we take $\gamma_0 \rightarrow 0$ (red region is Fig. 2a). Eventually, after a time $t_d = \Delta_d^{-1}$, the dissipation peak starts to decay at a rate Δ_d (blue area in Fig. 2a), where the gap $\Delta = \Delta_d = \varepsilon \gamma_0 L^{\alpha+1}$ closes as $L \rightarrow \infty$ (see Fig. 2b). The timescale t_d up to which the ramp survives is parametrically larger than the Thouless time (and, in particular, diverges in the thermodynamic limit), showing that the ramp of the closed RPM, which signals the chaotic correlations of the system, is robust against the addition of small amounts of dissipation to the system.

The robustness of the ramp persists for any $\alpha < -1$, but is destroyed by logarithmic corrections in the limit $\alpha \rightarrow -1^-$. Indeed, when the timescales of the Thouless and dissipation peaks become comparable, $t_{\text{DW}} \sim t_d$, i.e., $\gamma \sim 1/(L \log L) =: \gamma_{\text{ramp}}$, the ramp ceases to exist. Thus, when $\gamma \gtrsim \gamma_{\text{ramp}}$ (but still $\alpha < -1$), the two peaks have an overlap, and as a result the DFF shows a two-stage relaxation that is divided by the timescale t_{DW} : when $t \lesssim t_{\text{DW}}$ the exponent of the (exponential) decay is given by $\Delta_{\text{DW}} = 2\varepsilon$, whereas when $t \gtrsim t_{\text{DW}}$ the decay is dictated by the gap Δ_d . This is the intermediate regime where dissipation is strong enough to suppress the ramp completely but not enough to overwhelm the domain-wall contribution.

Anomalous relaxation.—As we increase the value of α , the system enters into another scaling regime with $-1 \leq \alpha \leq 0$. In this case, the gap Δ does not close and remains a positive finite constant as $L \rightarrow \infty$ (see Fig. 2b). Because t_* now goes to zero in the thermodynamic limit, the first term in $K_{\text{DW}}(t)$ is always dominant after $t_{\text{DW}} \approx t_{\text{Th}}/(2+\gamma)$ (the dotted line separating the green and yellow regions in Fig. 2a ceases to be constant). The most dramatic change, however, is that the gap, Eq. (4), changes as the dissipation peak is completely engulfed by the Thouless peak, which happens when $\Delta_d = \Delta_{\text{DW}}$, i.e., $\gamma = 2/L$ (corresponding to the dashed line separating the blue and yellow regions in Fig. 2a). That is, at $\alpha = -1$, as a function of γ_0 , the gap changes from $\Delta = \Delta_d = \varepsilon \gamma_0$ to $\Delta = \Delta_{\text{DW}} = \varepsilon(2+\gamma_0/L)$ (see left inset of Fig. 2b). Interestingly, from that point on, and also for all $-1 < \alpha < 0$, the gap is effectively independent of the dissipation strength γ_0 at large L , $\Delta = \Delta_{\text{DW}} = 2\varepsilon$. For $\alpha = 0$, it depends again on γ_0 , increasing linearly from its initial value, $\Delta = \varepsilon(2+\gamma_0)$ (see right inset of Fig. 2b). Finally, when $\alpha > 0$, the effect of the dissipation peak becomes completely negligible and the decay is solely controlled by the Thouless peak. The gap $\Delta_{\text{DW}} = \varepsilon(2+\gamma_0 L^\alpha) \approx \varepsilon \gamma_0 L^\alpha$ diverges in the thermodynamic limit (see Fig. 2b).

From the previous discussion, it follows that if $\alpha > -1$, the gap does not vanish in the dissipationless limit $\gamma_0 \rightarrow 0$ (as one would naively expect), provided that the thermodynamic limit $L \rightarrow \infty$ is taken first. This remarkable non-commutativity of limits implies that the system relaxes at a finite (or even diverging) rate even in the absence of an explicit coupling to the bath. In particular, for $-1 < \alpha < 0$, the gap is independent of γ_0 , and the relaxation is, therefore, driven not by the dissipation but instead by domain walls, which are one of the major consequences of the interplay between locality and the underlying RMT structure in Floquet many-body systems without conservation laws [25, 34]. A similar chaos-driven relaxation was first observed [68, 69] in the weak-dissipation regime dissipative Sachdev-Ye-Kitaev model [56, 68, 69, 73, 74] and dubbed *anomalous relaxation* [69]. It was conjectured to be a generic feature of chaotic quantum systems and has been, since then, observed in other strongly interacting dissipative systems, namely, a dissipative spin liquid [70] and the dephasing kicked Ising chain [71].

Purity.—Having seen that the DFF unveils a rich relaxation mechanism in the DRPM caused by the competition between quantum chaos and dissipation, it is natural to ask what kind of signatures of dissipative quantum chaos could be displayed in other quantities. Motivated by this, next, we look into the (ensemble-averaged) purity $\mathcal{P}_A(t)$. Let $A = \{1, \dots, L_A\}$ be the left part of the system and trace out its complement \bar{A} , yielding the reduced density matrix $\rho_A(t) = \text{Tr}_{\bar{A}}[\mathcal{W}^t[|\psi\rangle\langle\psi|]]$ where $|\psi\rangle$ is the initial product state. The purity is then defined

as $\mathcal{P}_A(t) = \exp\{-S_A^{(2)}\} = \text{Tr}_A[\rho_A(t)]^2$, where $S_A^{(n)}$ is the n th Rényi entropy, $S_A^{(n)} = \log(\text{Tr}[\rho_A(t)^n]/(1-n))$. The purity is expected to capture the time evolution of the strength of entanglement between A and \bar{A} . Without dissipation, $S_A^{(2)}$ in general grows linearly in time, causing the exponential decay of the purity. Again with the aid of diagrammatic techniques, we compute the ensemble-averaged purity $\overline{\mathcal{P}_A(t)}$ at large q (see the SM [72] for the derivation), obtaining the following simple expression

$$\overline{\mathcal{P}_A(t)} = e^{-2(1+\gamma L_A)\varepsilon t}. \quad (5)$$

We contrast this result with the previous computation of the DFF. At first sight, it would seem that anomalous relaxation is taking place, since the purity gap $2(1+\gamma L_A)\varepsilon$ does not close when $\gamma \rightarrow 0$ for any scaling with L_A . However, we recall that the purity gap is already finite, $\sim 2\varepsilon$, even in a close system and, thus, we are simply seeing the same relaxation enhanced by dissipation. We thus draw the important lesson that dissipative quantum chaos does not leave the same imprint in the relaxation of all quantities, and a judicious choice of observable is necessary.

Conclusions.—We have introduced the dissipative random phase model and studied its dissipative form factor and bipartite purity. We found that the interplay of depolarization and quantum chaos gives rise to intriguing behaviors during relaxation, which change dramatically as the scaling of the dissipation strength in the system size varies. Interestingly, one signature of quantum chaos in the spectral form factor, i.e., the late-time ramp, is robust against weak dissipation and its remnant persists over a timescale controlled by the gap. We also showed that the gap does not necessarily close in the thermodynamic limit even when the dissipation strength is sent to zero. Since quantum-channel circuits are realistic models of noisy intermediate-scale quantum (NISQ) computers and our results are largely independent of the precise choice of channel, it would be interesting to look for these signatures of dissipative quantum chaos experimentally in NISQ devices, using, e.g., an extension of the protocol proposed in Ref. [75].

Moreover, we expect the present Letter to stimulate a systematic study of open random quantum circuits, opening up several new directions in the study of dissipative quantum chaos. One outstanding task is to understand the precise nature of anomalous relaxation, and in particular, the extent to which it is universal in dissipative quantum chaotic systems [68–71]. Recently, in Ref. [71] the absence of anomalous relaxation in Hamiltonian systems was attributed to the presence of conservation laws, and it would be illuminating to study open Floquet many-body systems with conservation laws [30] to better appreciate the relation between conservation laws and anomalous relaxation. Another natural question to ask is how dissipative chaos could affect operator

dynamics, e.g., operator growth [22]. Besides establishing a regime of robustness of quantum chaotic features in the presence of dissipation, our results also pave the way toward a better understanding of the dynamical content of spectral correlations in non-Hermitian quantum systems.

Acknowledgements.—TY thanks Hosho Katsura for discussions out of which this work grew, and J. T. Chalker and S. J. Garratt for collaboration on a related topic. LS was supported by a Research Fellowship from the Royal Commission for the Exhibition of 1851 and by Fundação para Ciência e a Tecnologia (FCT-Portugal) through grant No. SFRH/BD/147477/2019. TY and LS acknowledge hospitality and support from the Simons Center for Geometry and Physics and the program “Fluctuations, Entanglements, and Chaos: Exact Results”, where this work was initiated. This project was partially funded within the QuantERA II Programme that has received funding from the European Union’s Horizon 2020 research and innovation programme under Grant Agreement No. 101017733 [76].

* takato.yoshimura@physics.ox.ac.uk

† lucas.seara.sa@tecnico.ulisboa.pt

- [1] M. Rigol, V. Dunjko, and M. Olshanii, Thermalization and its mechanism for generic isolated quantum systems, *Nature* **452**, 854 (2008).
- [2] L. D’Alessio, Y. Kafri, A. Polkovnikov, and M. Rigol, From quantum chaos and eigenstate thermalization to statistical mechanics and thermodynamics, *Adv. Phys.* **65**, 239 (2016).
- [3] K. A. Landsman, C. Figgatt, T. Schuster, N. M. Linke, B. Yoshida, N. Y. Yao, and C. Monroe, Verified quantum information scrambling, *Nature* **567**, 61 (2019).
- [4] M. S. Blok, V. V. Ramasesh, T. Schuster, K. O’Brien, J. M. Kreikebaum, D. Dahlen, A. Morvan, B. Yoshida, N. Y. Yao, and I. Siddiqi, Quantum Information Scrambling on a Superconducting Qutrit Processor, *Phys. Rev. X* **11**, 021010 (2021).
- [5] X. Mi, P. Roushan, C. Quintana, S. Mandra, J. Marshall, C. Neill, F. Arute, K. Arya, J. Atalaya, R. Babush, *et al.*, Information scrambling in quantum circuits, *Science* **374**, 1479 (2021).
- [6] P. Hayden and J. Preskill, Black holes as mirrors: quantum information in random subsystems, *J. High Energy Phys.* **2007**, 120 (2007).
- [7] Y. Sekino and L. Susskind, Fast scramblers, *J. High Energy Phys.* **2008**, 065 (2008).
- [8] J. Maldacena, S. H. Shenker, and D. Stanford, A bound on chaos, *J. High Energy Phys.* **2016**, 106 (2016).
- [9] J. S. Cotler, G. Gur-Ari, M. Hanada, J. Polchinski, P. Saad, S. H. Shenker, D. Stanford, A. Streicher, and M. Tezuka, Black holes and random matrices, *J. High Energy Phys.* **2017**, 118 (2017).
- [10] M. L. Mehta, *Random matrices* (Elsevier, New York, 2004).
- [11] L. Leviandier, M. Lombardi, R. Jost, and J. P. Pique,

- Fourier Transform: A Tool to Measure Statistical Level Properties in Very Complex Spectra, *Phys. Rev. Lett.* **56**, 2449 (1986).
- [12] E. Brézin and S. Hikami, Spectral form factor in a random matrix theory, *Phys. Rev. E* **55**, 4067 (1997).
- [13] R. E. Prange, The Spectral Form Factor Is Not Self-Averaging, *Phys. Rev. Lett.* **78**, 2280 (1997).
- [14] H. Gharibyan, M. Hanada, S. H. Shenker, and M. Tezuka, Onset of random matrix behavior in scrambling systems, *J. High Energy Phys.* **2018**, 124 (2018).
- [15] M. V. Berry, Semiclassical theory of spectral rigidity, *Proc. R. Soc. London A* **400**, 229 (1985).
- [16] M. Sieber and K. Richter, Correlations between periodic orbits and their rôle in spectral statistics, *Phys. Scr.* **2001**, 128 (2001).
- [17] M. Sieber, Leading off-diagonal approximation for the spectral form factor for uniformly hyperbolic systems, *J. Phys. A* **35**, L613 (2002).
- [18] S. Heusler, S. Müller, P. Braun, and F. Haake, Universal spectral form factor for chaotic dynamics, *J. Phys. A* **37**, L31 (2004).
- [19] S. Müller, S. Heusler, P. Braun, F. Haake, and A. Altland, Semiclassical Foundation of Universality in Quantum Chaos, *Phys. Rev. Lett.* **93**, 014103 (2004).
- [20] S. Müller, S. Heusler, P. Braun, F. Haake, and A. Altland, Periodic-orbit theory of universality in quantum chaos, *Phys. Rev. E* **72**, 046207 (2005).
- [21] P. Kos, M. Ljubotina, and T. Prosen, Many-Body Quantum Chaos: Analytic Connection to Random Matrix Theory, *Phys. Rev. X* **8**, 021062 (2018).
- [22] A. Nahum, S. Vijay, and J. Haah, Operator Spreading in Random Unitary Circuits, *Phys. Rev. X* **8**, 021014 (2018).
- [23] C. W. von Keyserlingk, T. Rakovszky, F. Pollmann, and S. L. Sondhi, Operator Hydrodynamics, OTOCs, and Entanglement Growth in Systems without Conservation Laws, *Phys. Rev. X* **8**, 021013 (2018).
- [24] A. Chan, A. De Luca, and J. T. Chalker, Solution of a Minimal Model for Many-Body Quantum Chaos, *Phys. Rev. X* **8**, 041019 (2018).
- [25] A. Chan, A. De Luca, and J. T. Chalker, Spectral Statistics in Spatially Extended Chaotic Quantum Many-Body Systems, *Phys. Rev. Lett.* **121**, 060601 (2018).
- [26] T. Rakovszky, F. Pollmann, and C. W. von Keyserlingk, Diffusive Hydrodynamics of Out-of-Time-Ordered Correlators with Charge Conservation, *Phys. Rev. X* **8**, 031058 (2018).
- [27] V. Khemani, A. Vishwanath, and D. A. Huse, Operator Spreading and the Emergence of Dissipative Hydrodynamics under Unitary Evolution with Conservation Laws, *Phys. Rev. X* **8**, 031057 (2018).
- [28] B. Bertini, P. Kos, and T. Prosen, Exact Spectral Form Factor in a Minimal Model of Many-Body Quantum Chaos, *Phys. Rev. Lett.* **121**, 264101 (2018).
- [29] B. Bertini, P. Kos, and T. Prosen, Exact Correlation Functions for Dual-Unitary Lattice Models in $1 + 1$ Dimensions, *Phys. Rev. Lett.* **123**, 210601 (2019).
- [30] A. J. Friedman, A. Chan, A. De Luca, and J. T. Chalker, Spectral Statistics and Many-Body Quantum Chaos with Conserved Charge, *Phys. Rev. Lett.* **123**, 210603 (2019).
- [31] A. Chan, A. De Luca, and J. T. Chalker, Eigenstate correlations, thermalization, and the butterfly effect, *Phys. Rev. Lett.* **122**, 220601 (2019).
- [32] M. P. Fisher, V. Khemani, A. Nahum, and S. Vijay, Random quantum circuits, *Annu. Rev. Condens. Matter Phys.* **14**, 335 (2023).
- [33] F. Arute, K. Arya, R. Babbush, D. Bacon, J. C. Bardin, R. Barends, R. Biswas, S. Boixo, F. G. Brandao, D. A. Buell, *et al.*, Quantum supremacy using a programmable superconducting processor, *Nature* **574**, 505 (2019).
- [34] S. J. Garratt and J. T. Chalker, Local Pairing of Feynman Histories in Many-Body Floquet Models, *Phys. Rev. X* **11**, 021051 (2021).
- [35] A. Chan, A. De Luca, and J. T. Chalker, Spectral Lyapunov exponents in chaotic and localized many-body quantum systems, *Phys. Rev. Res.* **3**, 023118 (2021).
- [36] Y. Li, X. Chen, and M. P. A. Fisher, Quantum Zeno effect and the many-body entanglement transition, *Phys. Rev. B* **98**, 205136 (2018).
- [37] A. Chan, R. M. Nandkishore, M. Pretko, and G. Smith, Unitary-projective entanglement dynamics, *Phys. Rev. B* **99**, 224307 (2019).
- [38] B. Skinner, J. Ruhman, and A. Nahum, Measurement-Induced Phase Transitions in the Dynamics of Entanglement, *Phys. Rev. X* **9**, 031009 (2019).
- [39] Y. Bao, S. Choi, and E. Altman, Theory of the phase transition in random unitary circuits with measurements, *Phys. Rev. B* **101**, 104301 (2020).
- [40] C.-M. Jian, Y.-Z. You, R. Vasseur, and A. W. W. Ludwig, Measurement-induced criticality in random quantum circuits, *Phys. Rev. B* **101**, 104302 (2020).
- [41] M. J. Gullans and D. A. Huse, Dynamical Purification Phase Transition Induced by Quantum Measurements, *Phys. Rev. X* **10**, 041020 (2020).
- [42] M. Ippoliti, M. J. Gullans, S. Gopalakrishnan, D. A. Huse, and V. Khemani, Entanglement Phase Transitions in Measurement-Only Dynamics, *Phys. Rev. X* **11**, 011030 (2021).
- [43] L. Sá, P. Ribeiro, T. Can, and T. Prosen, Spectral transitions and universal steady states in random Kraus maps and circuits, *Phys. Rev. B* **102**, 134310 (2020).
- [44] L. Sá, P. Ribeiro, and T. Prosen, Integrable nonunitary open quantum circuits, *Phys. Rev. B* **103**, 115132 (2021).
- [45] K. Noh, L. Jiang, and B. Fefferman, Efficient classical simulation of noisy random quantum circuits in one dimension, *Quantum* **4**, 318 (2020).
- [46] O. E. Sommer, F. Piazza, and D. J. Luitz, Many-body hierarchy of dissipative timescales in a quantum computer, *Phys. Rev. Res.* **3**, 023190 (2021).
- [47] Z. Weinstein, Y. Bao, and E. Altman, Measurement-Induced Power-Law Negativity in an Open Monitored Quantum Circuit, *Phys. Rev. Lett.* **129**, 080501 (2022).
- [48] Z. Li, S. Sang, and T. H. Hsieh, Entanglement dynamics of noisy random circuits, *Phys. Rev. B* **107**, 014307 (2023).
- [49] B. C. Dias, D. Perković, M. Haque, P. Ribeiro, and P. A. McClarty, Quantum noise as a symmetry-breaking field, *Phys. Rev. B* **108**, L060302 (2023).
- [50] Y. Li and M. Claassen, Statistical mechanics of monitored dissipative random circuits, *Phys. Rev. B* **108**, 104310 (2023).
- [51] P. Kos and G. Styliaris, Circuits of space and time quantum channels, *Quantum* **7**, 1020 (2023).
- [52] T. Van Vu, T. Kuwahara, and K. Saito, Universal fidelity-dissipation relations in quantum gates, [arXiv:2311.15762](https://arxiv.org/abs/2311.15762) (2023).
- [53] A. A. Patel, D. Chowdhury, S. Sachdev, and B. Swingle, Quantum butterfly effect in weakly interacting diffusive

- metals, *Phys. Rev. X* **7**, 031047 (2017).
- [54] D. A. Roberts and D. Stanford, Diagnosing chaos using four-point functions in two-dimensional conformal field theory, *Phys. Rev. Lett.* **115**, 131603 (2015).
- [55] T. Can, Random Lindblad dynamics, *J. Phys. A* **52**, 485302 (2019).
- [56] K. Kawabata, A. Kulkarni, J. Li, T. Numasawa, and S. Ryu, Dynamical quantum phase transitions in Sachdev-Ye-Kitaev Lindbladians, *Phys. Rev. B* **108**, 075110 (2023).
- [57] D. Braun, *Dissipative Quantum Chaos and Decoherence* (Springer, Heidelberg, 2001).
- [58] Y. V. Fyodorov, B. A. Khoruzhenko, and H.-J. Sommers, Almost Hermitian Random Matrices: Crossover from Wigner-Dyson to Ginibre Eigenvalue Statistics, *Phys. Rev. Lett.* **79**, 557 (1997).
- [59] J. Li, T. Prosen, and A. Chan, Spectral Statistics of Non-Hermitian Matrices and Dissipative Quantum Chaos, *Phys. Rev. Lett.* **127**, 170602 (2021).
- [60] A. M. García-García, L. Sá, and J. J. M. Verbaarschot, Universality and its limits in non-Hermitian many-body quantum chaos using the Sachdev-Ye-Kitaev model, *Phys. Rev. D* **107**, 066007 (2023).
- [61] S. Shivam, A. De Luca, D. A. Huse, and A. Chan, Many-Body Quantum Chaos and Emergence of Ginibre Ensemble, *Phys. Rev. Lett.* **130**, 140403 (2023).
- [62] S. Ghosh, S. Gupta, and M. Kulkarni, Spectral properties of disordered interacting non-Hermitian systems, *Phys. Rev. B* **106**, 134202 (2022).
- [63] A. Chan, S. Shivam, D. A. Huse, and A. De Luca, Many-body quantum chaos and space-time translational invariance, *Nat. Commun.* **13**, 7484 (2022).
- [64] Z. Xu, L. P. Garcia-Pintos, A. Chenu, and A. del Campo, Extreme Decoherence and Quantum Chaos, *Phys. Rev. Lett.* **122**, 014103 (2019).
- [65] Z. Xu, A. Chenu, T. Prosen, and A. del Campo, Thermofield dynamics: Quantum chaos versus decoherence, *Phys. Rev. B* **103**, 064309 (2021).
- [66] J. Cornelius, Z. Xu, A. Saxena, A. Chenu, and A. del Campo, Spectral Filtering Induced by Non-Hermitian Evolution with Balanced Gain and Loss: Enhancing Quantum Chaos, *Phys. Rev. Lett.* **128**, 190402 (2022).
- [67] A. S. Matsoukas-Roubeas, T. Prosen, and A. del Campo, Quantum Chaos and Coherence: Random Parametric Quantum Channels, [arXiv:2305.19326](https://arxiv.org/abs/2305.19326) (2023).
- [68] L. Sá, P. Ribeiro, and T. Prosen, Lindbladian dissipation of strongly-correlated quantum matter, *Phys. Rev. Res.* **4**, L022068 (2022).
- [69] A. M. García-García, L. Sá, J. J. M. Verbaarschot, and J. P. Zheng, Keldysh wormholes and anomalous relaxation in the dissipative Sachdev-Ye-Kitaev model, *Phys. Rev. D* **107**, 106006 (2023).
- [70] H. Shackleton and M. S. Scheurer, An exactly solvable dissipative spin liquid, [arXiv:2307.05743](https://arxiv.org/abs/2307.05743) (2023).
- [71] T. Mori, Liouvillian-gap analysis of open quantum many-body systems in the weak dissipation limit, [arXiv:2311.10304](https://arxiv.org/abs/2311.10304) (2023).
- [72] See the Supplemental Material for details on the diagrammatic computation of the DFF and purity.
- [73] A. Kulkarni, T. Numasawa, and S. Ryu, Lindbladian dynamics of the Sachdev-Ye-Kitaev model, *Phys. Rev. B* **106**, 075138 (2022).
- [74] A. M. García-García, L. Sá, J. J. M. Verbaarschot, and C. Yin, Emergent Topology in Many-Body Dissipative Quantum Chaos, [arXiv:2311.14640](https://arxiv.org/abs/2311.14640) (2023).
- [75] L. K. Joshi, A. Elben, A. Vikram, B. Vermersch, V. Galitski, and P. Zoller, Probing Many-Body Quantum Chaos with Quantum Simulators, *Phys. Rev. X* **12**, 011018 (2022).
- [76] DOI: 10.54499/QuantERA/0003/2021.

SUPPLEMENTARY MATERIAL FOR
 “ROBUSTNESS OF QUANTUM CHAOS AND ANOMALOUS RELAXATION IN
 OPEN QUANTUM CIRCUITS”

Takato Yoshimura^{1,2} and Lucas Sá^{3,4}

¹All Souls College, Oxford OX1 4AL, U.K.

²Rudolf Peierls Centre for Theoretical Physics, University of Oxford, 1 Keble Road, Oxford OX1
3NP, U.K.

³TCM Group, Cavendish Laboratory, University of Cambridge, JJ Thomson Avenue, Cambridge
CB3 0HE, U.K.

⁴CeFEMA, Instituto Superior Técnico, Universidade de Lisboa, Av. Rovisco Pais, 1049-001
Lisboa, Portugal

I. DIAGRAMMATIC COMPUTATION OF THE DISSIPATIVE FORM FACTOR

A. Haar averaging in the presence of dissipation

The computation of the DFF proceeds similarly to that of the standard SFF [1]. We first Haar-average each on-site diagram, which induces local pairings among on-site unitaries. We then enumerate the weight of every contributing local pairing at large q and analyze what phase contribution we get upon averaging with respect to the phase φ for every possible pair of two pairings on two neighboring sites. This gives rise to the transfer matrix \hat{T} of the DFF, which allows us to compute the DFF as $\overline{F(t)} = \text{Tr} \hat{T}^L$.

Let us start with the Haar average at site $n = 1, \dots, L$. It is useful to represent on-site diagrams as in Fig. S1, where we depict the case of $t = 3$ (it corresponds to a rotation around a vertical axis of the diagram of Fig. 1a of the Main Text) and time runs upward. Squares represent the on-site quantum channels $M_{j_x\tau}$ and $M_{j_x\tau}^*$, whereas circles are the unitaries that are contracted after Haar averaging (contractions are denoted by dashed lines). Haar averaging then amounts to $(t!)^2$ different pairings of indices of unitaries U_n and U_n^* [1]. It turns out that, as in the SFF, the leading pairings are those corresponding to cyclic pairings of the set of U_n and U_n^* . Namely, when

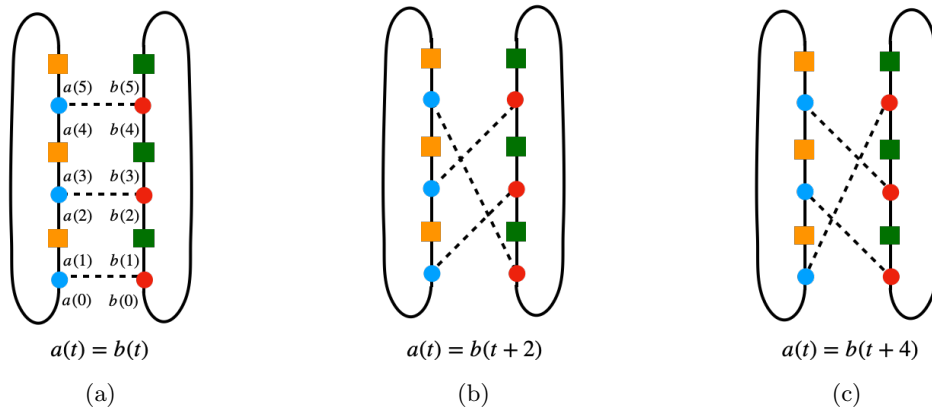


FIG. S1. Diagrammatic representation of the leading contributions to the DFF as $q \rightarrow \infty$. Blue and red circles represent U_n and U_n^* , while yellow and green squares denote the Kraus operators M_j and M_j^* . The dashed lines denote contractions of unitaries. $a(\tau)$ and $b(\tau)$ denote the indices of the unitaries U_n and U_n^* , respectively (e.g., the first unitary has U_n has indices $[U_n]_{a(0),a(1)}$). The three diagrams depict the leading cyclic pairings at $t = 3$, corresponding to (a) $a(t) = b(t)$, (b) $a(t) = b(t + 2)$, and (c) $a(t) = b(t + 4)$.

expanding the DFF in the computational spin basis at site n , we have the Haar average

$$\overline{[U_n]_{a(0),a(1)} \cdots [U_n]_{a(2t-4),a(2t-3)} [U_n]_{a(2t-2),a(2t-1)} [U_n^*]_{b(0),b(1)} \cdots [U_n^*]_{b(2t-4),b(2t-3)} [U_n^*]_{b(2t-2),b(2t-1)}}, \quad (\text{S1})$$

where we note that the phase coupling acts diagonally in this basis and that, unlike in the computation of the SFF, there is no overlap of indices as a Kraus operator is acting on the state after every unitary. Haar averaging then yields cyclic pairings of indices labeled by $a(t) = b(t + 2s)$ for $s = 0, \dots, t - 1$ [with the periodic condition that $a(2t) = a(0)$] as the leading contributions at $q \rightarrow \infty$. See Fig. S1 for the cyclic-pairing diagrams at $t = 3$.

The difference between the SFF and the DFF, however, is that in the DFF all $s \neq 0$ pairings are suppressed compared to the $s = 0$ pairing. Indeed, the $s = 0$ pairing has weight 1, while all $s \neq 0$ pairings have the same weight smaller than 1. For instance, it is readily seen that the $s = 1$ and $s = 2$ pairings represented by Fig. S1b and S1c have the weight

$$q^{-3} \sum_{i,j,k} \text{Tr} M_i M_j^\dagger \text{Tr} M_j M_k^\dagger \text{Tr} M_k M_i^\dagger = \sum_{i,j,k} \eta_i \delta_{ij} \eta_j \delta_{jk} \eta_k \delta_{ki} = \sum_i \eta_i^3. \quad (\text{S2})$$

In general, for arbitrary t the weight is simply given by $\kappa = \sum_{i=0}^{k-1} \eta_i^t$, which reduces to $(1 - p)^t$ when the system is dissipated by depolarizing channels. In contrast, the $s = 0$ pairing in Fig. S1a yields

$$q^{-3} \sum_{i,j,k} \text{Tr} M_i M_i^\dagger \text{Tr} M_j M_j^\dagger \text{Tr} M_k M_k^\dagger = \left(\sum_i \eta_i \right)^3 = 1. \quad (\text{S3})$$

Next, we move on to build the transfer matrix. This can be done by performing phase averaging on neighboring sites for every possible pairing. The situation is again the same as in the SFF in that if two sites have different pairings then the resulting phase is $e^{-\varepsilon t}$ [1]. We thus have the transfer matrix of the form $T = (1 - e^{-\varepsilon t})I + e^{-\varepsilon t}E$ together with the on-site matrix D that encodes different weights in $s = 0$ and $s \neq 0$ pairings. For instance, when $t = 3$ they are given by

$$T = \begin{pmatrix} 1 & e^{-3\varepsilon} & e^{-3\varepsilon} \\ e^{-3\varepsilon} & 1 & e^{-3\varepsilon} \\ e^{-3\varepsilon} & e^{-3\varepsilon} & 1 \end{pmatrix}, \quad D = \begin{pmatrix} 1 & 0 & 0 \\ 0 & \sum_{i=0}^{k-1} \eta_i^3 & 0 \\ 0 & 0 & \sum_{i=0}^{k-1} \eta_i^3 \end{pmatrix}. \quad (\text{S4})$$

With these, we obtain the exact large- q DFF $\overline{F(t)} = \text{Tr}(TD)^L = \text{Tr}\hat{T}^L$.

While the large- q DFF we obtained in terms of the transfer matrix is exact at any t and for any system size, it is still analytically challenging to extract any information out of it. There are two situations for which we have analytic handles, to which we turn next.

B. Small system size

The first case is when L is not too large. In this case, the trace $\text{Tr}\hat{T}^L$ can be still computed by expressing the transfer matrix as

$$\hat{T} = \kappa T + (1 - \kappa)T|0\rangle\langle 0|. \quad (\text{S5})$$

This allows us to express the DFF as a sum of terms involving the SFF $\overline{K(t)} = \text{Tr}T^L$ and the partial SFF (PSFF)

$$\overline{K_A(t)} = q^{-(L-L_A)} \overline{\text{Tr}_A[(\text{Tr}_A W(t)^\dagger)(\text{Tr}_A W(t))]}, \quad (\text{S6})$$

where A is a subsystem of size L_A . It is a simple matter to observe that the PSFF at large q is given by $\overline{K_A(t)} = T_{00}^{L_A+1}$ [2].

For instance, for $L = 3$ and $L = 4$ we have

$$\begin{aligned} \overline{F_{L=3}(t)} &= \kappa^3 \overline{K(t)} + 3\kappa^2(1 - \kappa) \overline{K_2(t)} + 3\kappa(1 - \kappa)^2 \overline{K_1(t)} + (1 - \kappa)^3 \\ \overline{F_{L=4}(t)} &= \kappa^4 \overline{K(t)} + 4\kappa^3(1 - \kappa) \overline{K_3(t)} + \kappa^2(1 - \kappa)^2 \left(4\overline{K_2(t)} + 2[\overline{K_1(t)}]^2 \right) \\ &\quad + 4\kappa(1 - \kappa)^3 \overline{K_1(t)} + (1 - \kappa)^4, \end{aligned} \quad (\text{S7})$$

but it is clear that the computation becomes intractable as L increases.

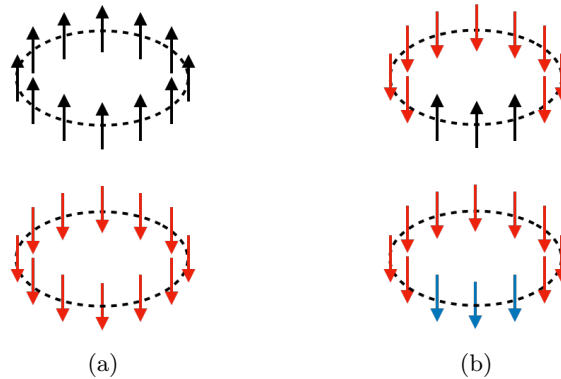


FIG. S2. Leading domain-wall configurations at late times. A down spin refers to one of the $s \neq 0$ pairings (different colors mean different pairings), whereas an up spin is a $s = 0$ pairing.

C. Domain-wall expansion

Although it is always useful to have an exact closed expression, in the present work, we are mainly interested in the relaxation of the DRPM, which is characterized by the late-time behavior of the DFF. In this case, we can organize the DFF, $\overline{F}(t) = \text{Tr} \hat{T}^L$, which is a sum of all the pairing configurations with periodic boundary conditions, in terms of domain walls of local pairings labeled by $s = 0, \dots, t-1$. Here what we call a domain wall is simply a configuration of two different pairings on two neighboring sites. Note that periodic boundary conditions allow only an even number of domain walls. Since each domain wall carries the entropic cost $e^{-\varepsilon t}$, the more domain walls we have in a pairing configuration, the less contribution it has at late times. This implies that the late-time behavior of the DFF is controlled by 1) pairing configurations without any domain wall and 2) those with only two domain walls.

Let us start with the first case. The absence of domain walls means that every site hosts the same pairing. Noting that while $s = 0$ pairing carries the factor 1 the other $s \neq 0$ pairings come with κ , and, thus, the contributions from these configurations are $1 + (t-1)\kappa^L$ as depicted in Fig. S2a.

Instead, when we have two domain walls, they divide the system into two regions, each of which is made of a fixed pairing. We can further classify them into two categories: the first type of configurations consists of one region with $s = 0$ pairings and another region with one of $s \neq 0$ pairings (see the upper panel in Fig. S2b), and the second type of configurations is fully made of $s \neq 0$ pairings but in each region a different one is used (e.g., $s = 1$ pairing in one region and $s = 2$ in another, see the lower panel in Fig. S2b).

Contributions from the first type can be obtained by noting that the region with $s \neq 0$ pairings could be allocated to the system in $L - a + 1$ different positions where a is the size of the $s \neq 0$ pairing region, and there are $t - 1$ possible pairings. We thus have a contribution

$$(t - 1) \sum_{a=1}^L (L - a + 1) \kappa^a e^{-2\epsilon t} = (t - 1) \frac{L - (L + 1)\kappa + \kappa^{L+1}}{(1 - \kappa)^2} \kappa e^{-2\epsilon t}. \quad (\text{S8})$$

Likewise, we can also evaluate the contributions from the second type, which gives

$$\frac{(t - 1)(t - 2)}{2} \frac{L(L - 1)}{2} \kappa^L e^{-2\epsilon t}. \quad (\text{S9})$$

Combining these, the late-time asymptotics of the DFF has the following form:

$$\overline{F(t)} \simeq 1 + t\kappa^L + tL\kappa e^{-2\epsilon t} + \frac{t^2 L^2}{4} \kappa^L e^{-2\epsilon t}, \quad (\text{S10})$$

where we used the fact that, at late times, $\kappa \ll 1$.

II. DIAGRAMMATIC COMPUTATION OF THE PURITY

While we have four replicas of W and W^\dagger in the purity, its computation can be carried out following the same idea as in the DFF. Again we start with representing the purity $\mathcal{P}_A(t)$ diagrammatically. In particular, we express it using the “folded” picture [3] as in Fig. S3a, where the purity at $t = 2$ in the system of size $L = 4$ with $L_A = 2$ is depicted. Note the different boundary conditions on A and \bar{A} , which amounts to different shapes of on-site diagrams on A and \bar{A} as shown in Fig. S3b and S3c. It turns out that each diagram in Fig. S3b and S3c has a unique contributing pairing at large q , which is indicated in these diagrams. In particular, at $t = 2$, the value of the leading pairing on A is

$$q^{-4} \sum_{i,j,k,l} \text{Tr} M_i M_j^\dagger \text{Tr} M_j M_i^\dagger \text{Tr} M_k M_l^\dagger \text{Tr} M_l M_k^\dagger = \left(\sum_i \eta_i^2 \right)^2, \quad (\text{S11})$$

whereas on \bar{A} the weight is simply 1 (here, we normalized the initial product state as $|\langle \psi | \psi \rangle|^2 = 1$). For general t , it can be readily inferred that the weights are given by $(\sum_i \eta_i^2)^n$ and 1, respectively.

Since these two pairings are clearly different, phase averaging induces a single domain wall at the boundary of A and \bar{A} with the statistical cost $e^{-2\epsilon t}$ (the factor 2 is due to four replicas of the unitaries in the purity), whereas no domain wall is produced in the bulk of A and \bar{A} . Note that this structure is similar to what was observed in the purity of dissipationless random unitary circuits [4, 5]. Combining these observations, we arrive at the ensemble-averaged purity at large q :

$$\overline{\mathcal{P}(t)} = e^{-4\epsilon t} \left(\sum_i \eta_i^2 \right)^{nL_A}. \quad (\text{S12})$$

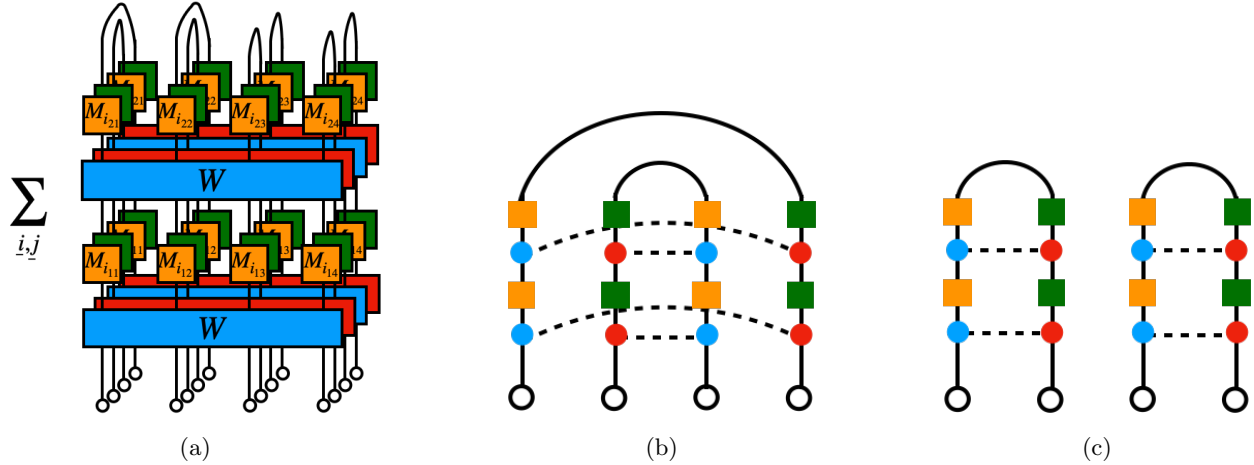


FIG. S3. (a) Purity in the folded picture at $t = 2$ and $L_A = L_{\bar{A}} = 2$. The empty circles at the bottom represent the initial product state $|\psi\rangle$. (b) and (c) show the leading pairings of on-site diagrams on A and \bar{A} at $t = 2$, respectively.

In the case of the depolarizing channel, it reduces to

$$\overline{\mathcal{P}(t)} = e^{-2(1+\gamma L_A)\epsilon t}. \quad (\text{S13})$$

-
- [1] A. Chan, A. De Luca, and J. T. Chalker, Spectral Statistics in Spatially Extended Chaotic Quantum Many-Body Systems, *Phys. Rev. Lett.* **121**, 060601 (2018).
 - [2] S. J. Garratt and J. T. Chalker, Local Pairing of Feynman Histories in Many-Body Floquet Models, *Phys. Rev. X* **11**, 021051 (2021).
 - [3] A. Chan, A. De Luca, and J. T. Chalker, Solution of a Minimal Model for Many-Body Quantum Chaos, *Phys. Rev. X* **8**, 041019 (2018).
 - [4] A. Nahum, J. Ruhman, S. Vijay, and J. Haah, Quantum Entanglement Growth under Random Unitary Dynamics, *Phys. Rev. X* **7**, 031016 (2017).
 - [5] T. Zhou and A. Nahum, Emergent statistical mechanics of entanglement in random unitary circuits, *Phys. Rev. B* **99**, 174205 (2019).